Advanced Ceramics Progress: Vol. 9, No. 1, (Winter 2023) 28-37

Materials and Energy Research Center
MERC

Contents lists available at ACERP

Advanced Ceramics Progress

Journal Homepage: www.acerp.ir

Original Research Article

$Zn_xCo_{3-x}O_4$ Hydrothermally Mesoporous Nanoparticles (ZCH): Structure, Optical, and Surface Analysis

Somayeh Rahimi [a], Behzad Koozegar Kaleji [b,*], Mahdi Kazazi [b]

[a] *MSc, Department of Materials Engineering, Faculty of Engineering, Malayer University, Malayer, Iran, P.O. Box 65719-9586*
[b] *Associate Professor, Department of Materials Engineering, Faculty of Engineering, Malayer University, Malayer, Iran, P.O. Box 65719-95863*

* Corresponding Author Email: b.kaleji@malayeru.ac.ir (B. Koozegar Kaleji) URL: https://www.acerp.ir/article_166443.html

ARTICLE INFO

Article History:

Received 2 January 2023
Received in revised form 26 January 2023
Accepted 6 February 2023

Keywords:

Cobalt Oxide Nanoparticles
Zn Content
Photocatalytic
Hydrothermal
Surface Analysis

ABSTRACT

In this research, cobalt oxide solid solution nanoparticles with different molar percentages of zinc content (2.5, 5, 7.5, 10, 15, 20, 30 mol %) were synthesized through hydrothermal method. Cobalt nitrate and zinc nitrate were used as the sources of cobalt oxide and zinc contents in this research. In order to investigate the structural properties, the chemical state, optical, photocatalytic properties as well as the microstructure of the synthesized nanoparticles were characterized based on the XRD, BET-BJH, UV-Vis, XPS, TEM, and FESEM analyzes. The results of the X-ray phase analysis showed that addition of this content to the structure of cobalt oxide led to a decrease in the crystal size. The crystallite sizes of the pure and doped samples were about 9.48 nm and about 8.8 nm, respectively. According to the FESEM images, the particle size of the pure sample was in the range of 20-40 nm, and that of the doped ZCH-300 sample (10 % Zn) in the range of 20-30 nm. The specific surface areas (BET) of the pure sample and the sample with 10 % zinc were about 75 m^2/g and 92 m^2/g, respectively. Compared to the pure CH nanoparticles Doped Co_3O_4 (CH), mesoporous nanoparticles were observed to have the highest photocatalytic activity. The photocatalytic analysis results showed that the highest degradation percentage of the solution, i.e., 10.6 ($\eta_{ZCH-300}$ = 10.6 %), was obtained in the presence of the doped sample with zinc cation (10 % Zn).

https://doi.org/10.30501/acp.2023.379335.1115

1. INTRODUCTION

Cobalt oxide (Co_3O_4) is a p-type semiconductor. In recent years, considerable attention has been draw to the photodegradation of color pollutants due to their low cost, excellent chemical, and physical stability [1]. Cobalt oxide nanomaterials are characterized by extraordinary optical, electrical, and magnetic properties [2] and are used for a variety of applications such as gas sensors [3], supercapacitors [4], lithium-ion batteries [5,6], and energy storage devices [7,8]. The behavior of nanoparticles depends on their structural morphology, specific surface area, and structural porosity. Nanoparticles can be prepared through different methods such as sol-gel, hydrothermal, and chemical reduction. Zhao et al. [9] investigated the Co_3O_4 nanostructures in the form of nanowires, nanorods, and spherical nanoparticles using the hydrothermal method to degrade methyl orange dye under ultraviolet radiation. Chen et al. studied the hollow microspheres of Co_3O_4 during a two-

Please cite this article as: Rahimi, S., Koozegar Kaleji, B., Kazazi, M., "$Zn_xCo_{3-x}O_4$ Hydrothermally Mesoporous Nanoparticles (ZCH): Structure, Optical, and Surface Analysis", ***Advanced Ceramics Progress***, Vol. 9, No. 1, (2023), 28-37. https://doi.org/10.30501/acp.2023.379335.1115

step process to degrade methyl orange dye under ultraviolet radiation [10]. The photocatalytic properties of Co_3O_4 are not suitable due to the high rate of electron-hole pair recombination in this structure. Further, some methods such as the particle size control [11] or morphology control [12,13], non-metallic dopant or metallic dopant such as Fluorine [14] and Manganese, Nickel or Manganese [15,16] were particularly investigated. Doping in the semiconductor fabrication is one of the methods that increases its photocatalytic performance. The purpose of doping is to improve the photocatalytic properties of nanoparticles. In a chemical co-precipitation method study, Hitkari et al. [16] investigated the effect of Cr dopant (1 and 5 %) on the physical properties of cobalt oxide nanoparticles. They reported that 5 % Cr in the structure of cobalt oxide had a better photocatalytic efficiency than the pure sample. The previous studies in this field were taken into account and to the best of the authors' knowledge, no research has been done on the hydrothermal synthesis of ZCH (Zn doped cobalt oxide) mesoporous nanoparticles so far. To this end, a series of Zn doped Co_3O_4 nanoparticles were prepared with different Zn contents (code: ZCH-2.5 % Zn, ZCH-5 % Zn, ZCH-7.5 % Zn, ZCH-10 % Zn, ZCH-15 % Zn, ZCH-20 % Zn, and ZCH-30 % Zn).

The effect of the Zn content on the structural, photocatalytic, and optical properties of the synthesized Co_3O_4 mesoporous nanoparticles was also studied. In order to investigate the photocatalytic properties, the degradation of methylene blue dye solution under visible light irradiation in the presence of synthesized nanoparticles was taken into consideration.

2. MATERIALS AND METHODS

2.1. Raw Materials

In this research, Cobalt nitrate hexahydrate ($Co(NO_3)_2.6H_2O$), ammonium fluoride (NH_4F), and urea (CH_4N_2O) were used as the precursors materials. Zinc nitrate hexahydrate ($Zn(NO_3)_2.6H_2O$) was also used as the precursors of the Zn content. All the raw chemicals are analytical-grade reagents that were purchased from Merck Company and used as received without any further purification. In addition, organic methylene blue solution was used for photocatalytic activity.

2.2. Experimental Procedure

In this research, Co_3O_4 (CH) and doped (ZCH) samples of mesoporous nanoparticles were synthesized by a simple and facile hydrothermal route. Briefly, 60 ml of distilled water, 0.655 g (2.25 mmol) of $Co(NO_3)_2.6H_2O$, 0.676 g (11.25 mmol) CH_4N_2O, and 0.167 g (4.5 mmol) NH_4F were mixed together in beaker and magnetically stirred at 25 °C (R.T.) for 20 min.

The thoroughly mixed precursor was then transferred to a 100 ml Teflon-coated stainless-steel autoclave, which was thoroughly sealed and subsequently heated in an electric oven at 150 °C for four hours to precipitate. After cooling down to room temperature, the prepared precipitate was removed by centrifugation and washed three times with distilled water and absolute ethanol, respectively. Of course, after each centrifuge step, the precipitate was formed in ultrasonic for five minutes. The product was dried in air at 60 °C for 12 hours. Finally, the dried precipitate was calcined at 300 °C for two hours. Zn doped Co_3O_4 nanoparticles (ZCH) were obtained in the same process, except that an appropriate amount of $Zn(NO_3)_2.6H_2O$ was added as a source of Zn^{2+} ions (2.5, 5, 7.5, 10, 15, 20, and 30 % Zn).

2.3. Nanoparticle Characterization Methods

The synthesized samples were evaluated using different techniques. Phase analysis of the synthesized sample was performed using X-ray diffraction (XRD, Philips, MPD-XPERT with Cukα radiation, λ= 0.154 nm). The optical absorption spectra, photocatalytic degradation, and band gap energy (E_g) of the synthesized nanoparticles were measured using the spekol-2000 spectrophotometer in the wavelength range of 200-800 nm. The surface area and pore size distribution of the samples were determined by a BELSORP measuring instrument (BELSORP-mini, JAPAN, INC) using nitrogen gas adsorption-desorption technique at 77 K.

Later, X-ray Photoelectron Spectroscopy (XPS) measurements were performed on a VG ESCALAB 210 XPS system with Mg Kα (1253.6 eV) source. All the binding energies were referenced to the C 1s peak at 284.6 eV of the surface adventitious carbon. The morphology of the mesoporous nanopowders was studied using Field Emission Scanning Electron Microscopy (FESEM, MIRA3-TESCAN) with an accelerating voltage of 10-15 kV. High Resolution Transmission Electron Microscopy (HRTEM) was performed on a Jeol-JEM 2011 system operated at 200 kV.

2.4 Photocatalytic Activity

The photocatalytic degradation of organic pollutants by the samples was evaluated by the degradation of methylene blue (MB) as a model pollutant solution under visible (250 W) light irradiation. The photocatalytic experiment was carried out by taking 0.1 g of each sample in 50 ml MB solutions (10 ppm). Prior to the light irradiation, these solutions were magnetically stirred for 30 min in a dark place to achieve the adsorption-desorption equilibrium. The above solutions were irradiated with light and after every 20 min, a 3 ml sample of the solution was taken from which, the catalyst was separated by centrifugation to obtain a clear liquid. The photodegradation rates of the MB solution at the given intervals of irradiation was analyzed using a Ultraviolet–visible (UV-Vis) spectrophotometer. The degradation

percentage of MB, which represents the photocatalytic efficiency of the samples, can be determined by Equation (1).

$$\eta = [1-A_t/A_0]\times 100 \quad (1)$$

where η is the photocatalytic efficiency of MB, A_t the absorption after radiation, and A_0 the absorption before radiation [17].

The energy band gap corresponds to the absorption limit that can be roughly evaluated using the following equation:

$$E_g\ (eV) = 1240/\lambda_{edge} \quad (2)$$

where λ_{edge} represents the absorption limit of the semiconductor. Here, λ_{edge} can be extracted from the absorption spectrum by determining the first derivative of absorbance with respect to the wavelength near the absorption edge and finding the point at which the derivative spectrum reaches its minimum value**.** This point is in fact the reflection point of the absorption curve. The tangent line of the absorption curve at the reflection point intersects with the x-axis on which absorbance reaches 0 and indicates λ_{edge}.

3. RESULTS AND DISCUSSION

3.1. Phase Analysis of CH and ZCH Samples Calcined at 300 °C

The crystal structure and crystalline phases of the pure and doped samples with different percentages of Zn content were investigated using XRD analysis, the results of which are given in Figures 1 and 2. The crystal peaks at the diffraction angles (Figure 1) of 31.1°, 36.7°, 38.6°, 46.8°, 55.6°, 59.4°, and 65.2° are attributed to the crystal plates with Miller index, the (220), (311), (222), (400), (422), (511), and (440) planes of the cubic spinel Co_3O_4, respectively.

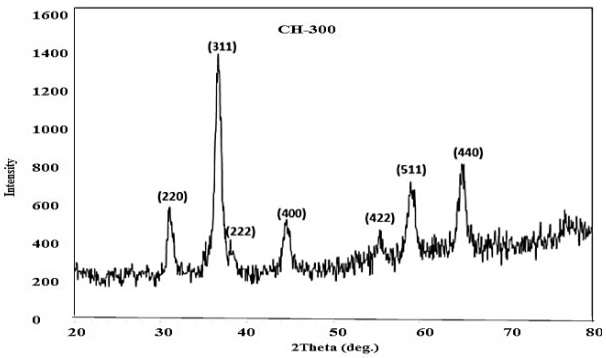

Figure 1. XRD pattern of pure Co_3O_4 (CH) sample after calcination at 300 °C for 2 h

The XRD pattern of all samples corresponds to the JCPDS card no.:43-1003 [18]. The peaks of the synthesized ZCH sample (Figure 2) in the presence of Zn content (solid solution up to 10 % Zn) are similar to those of the pure sample. In the doped samples, the crystal peaks shift to lower angles, which can be attributed to the ionic radius of Zn^{2+} (0.74 Å) which is larger than Co^{3+} (0.6 Å).

Followed by addition of Zn cation up to about 10 %, a peak shift to the lower angles in the Co_3O_4 lattice in the XRD results was observed; however, with the addition of a higher percentage of Zn cation (Zn > 10%), formation of a solid solution of Co_3O_4-ZnO was witnessed.

In the samples with lower than 10 %, no secondary crystallized phase (ZnO phase, JCPDS: 36-1451) were observed in the XRD patterns of the ZCH samples (Zn < 10 %), suggesting that the Zn ions were well incorporated into the Co_3O_4 lattice (Figure 2).

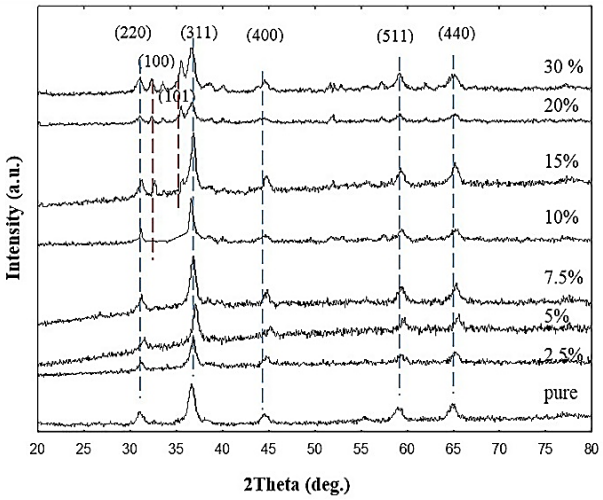

Figure 2. XRD patterns of $Zn_xCo_{3-x}O_4$ (ZCH) samples after calcination at 300 °C for 2 h (Blue Line: Co_3O_4, Red line: ZnO)

3.2. BET-BJH and XPS Analysis of CH and ZCH Nanoparticles

The specific surface area (BET) and porosity of the pure cobalt oxide (CH) sample and ZCH-300 (10 % Zn) calcined at 300 °C were investigated using nitrogen adsorption-desorption isotherm.

The hysteresis loop is compatible with type IV for both CH (Figure 3a) and ZCH (Figure 3c) samples according to the AUPAC classification which confirms mesoporous characteristic of the prepared samples. A comparison was further made between the two calcined samples at 300 °C and consequently, the values of the specific surface area (BET) for the CH sample were calculated as 75.1 m^2/g and 93.2 m^2/g for the ZCH sample, indicating that the sample in the presence of content had a smaller particle size than the pure sample. The shape of the pore is H4 type with a narrow opening porosity with uniform channels in the lattice where the structure of these

porosities is mesomatically porous. In the presence of Zn content (ZCH), these channels are arranged spherically and cylindrically, and the hysteresis loop represents the mesoporous material.

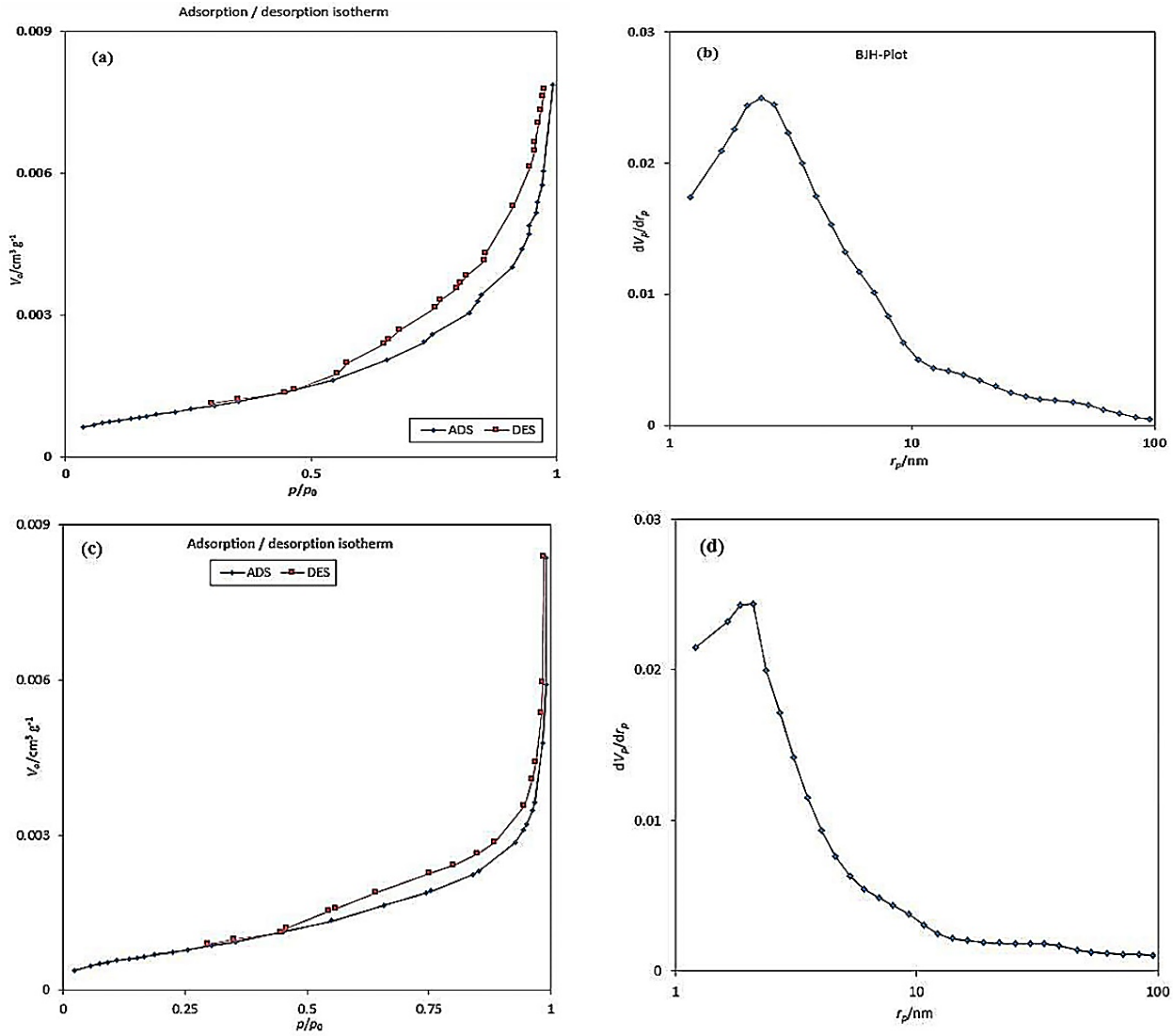

Figure 3. N2 physisorption isotherms (BET) and pore size distribution (BJH) of CH (a,b) and ZCH (c,d) hydrothermally mesoporous nanoparticles calcined at 300 °C

According to the BJH adsorption diagram (Figures 3b,d), the average pore diameters in the CH and ZCH sample are 14.8 nm and 14.2 nm, respectively. Of note, BJH curve for both samples (Figure 3b,d) include a high percentage of mesoporous particles with a small percentage of microporous and macro-porous particles [19]. XPS studies were carried out to determine the chemical composition, surface element composition, and chemical valance states of the synthesized samples. The results of these analyses are reported in Figure 4 on a wide scan. Figure 4a illustrates the broad-spectrum photoelectron spectrum of pure (CH-300) and doped (ZCH-300) samples. Figure 4a shows the presence of Co, Zn, O, and C elements. Figure 4b demonstrates the high-resolution Co 2p spectra. The peaks at 780 and 794.4 eV are attributed to the cobalt cation with the valences of 3 (Co^{3+}) and 2 (Co^{2+}) [20].

Figure 4c shows the high-resolution Zn 2p spectrum of the ZCH sample. The two peaks at 1044.8 and 1021.2 eV are attributed to Zn $2p_{1/2}$ and Zn $2p_{3/2}$, respectively, indicating the presence of a Zn cation with the valence of +2 (Zn^{2+}) [21].

The high-resolution O 1s spectrum in Figure 4d can be further subdivided into two suitable peaks at 530.5 eV and 531.6 eV, which confirm the presence of lattice oxygen (O_L:Co-O) and surface oxygen (O_H:O-H) on the surface [22]. The peaks of Co 2p, O 1s in the XPS spectrum of the ZCH compound are indicative of the

presence of oxygen vacancies, which is useful for the photocatalytic process because it leads to the separation of the electron-hole pair.

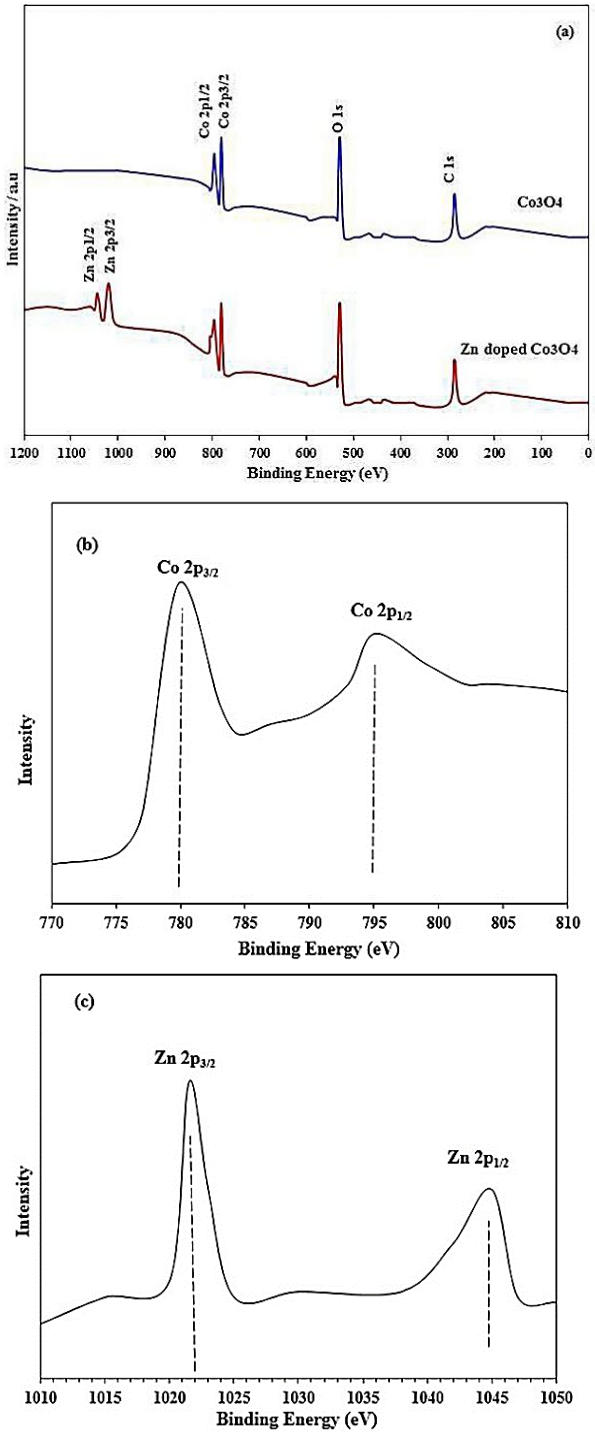

Figure 4. XPS spectra of the pure Co_3O_4 and Zn doped Co_3O_4 mesoporous nanoparticles, scanned in (a) Broad scan XPS analysis of Pure Co_3O_4 and Zn doped Co_3O_4 sample, high-resolution XPS spectra of (b) Co 2p, (c) Zn 2p, and (d) O 1s spectra for ZCH sample calcined at 300

3.3. UV-Vis analysis of CH and ZCH Samples

Photocatalytic degradation of methylene blue dye solution in the presence of the pure sample (CH) and samples with different percentages of Zn content (ZCH) were prepared for spectrophotometric analysis. The analysis results are reported in Figures 5a,b and Table 1.

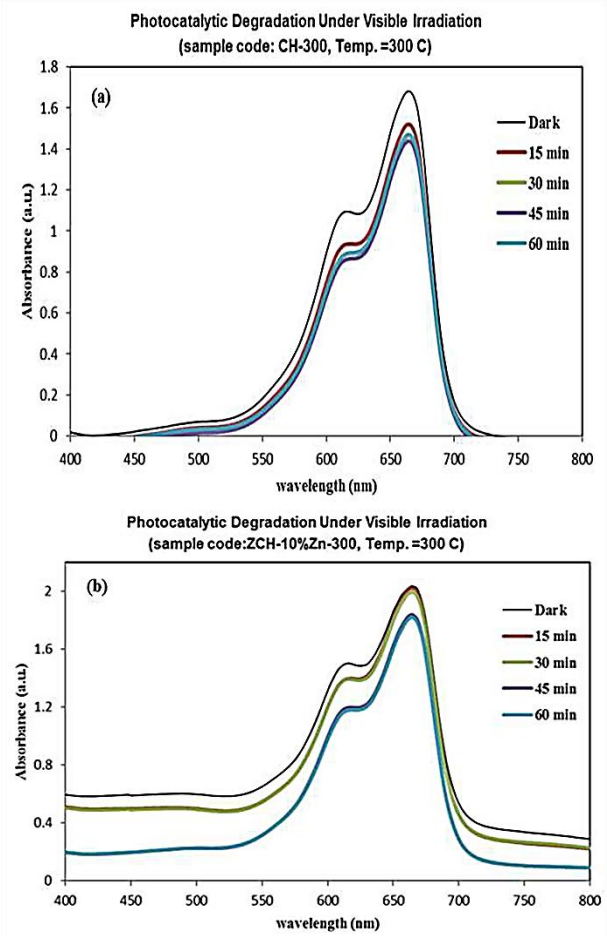

Figure 5. (a) Photocatalytic degradation spectra of CH-300 nanoparticles, (b) ZCH-300 nanoparticles under visible light irradiation time (1h)

TABLE 1. Photocatalytic activity of ZCH samples under visible light irradiation

Samples	η %
ZCH-2.5 %	5.25
ZCH-5 %	10.22
ZCH-7.5 %	6.62
ZCH-10 %	10.6
ZCH-15 %	3.34
ZCH-20 %	4.54
ZCH-30 %	5.29

Figure 5a shows the degradation of MB solution in the presence of pure cobalt oxide (CH-300) at 300 °C under visible light irradiation. The degradation percentage of

the MB dye solution at this temperature is about 12.7 %. The photocatlytic degradation in the presence of doped samples with different percentages of Zn cation was measured, and the UV-Vis spectrum of ZCH-10 % Zn sample was reported as one of the samples with higher photocatalytic efficiency than that of other samples with other percentages in Figure 5b. As observed in Figures 5a,b, after different irradiation times (t = 15, 30, 45, and 60 min), the amount of adsorption (A_t) in the solution decreases, indicating an increase in the photocatalytic efficiency under visible irradiation at different times.

The results of this test for all doped samples are reported in Table 1. The highest degradation percentage of the solution was obtained in the presence of the sample doped with zinc cation (10 % Zn) which was equal to 10.6. The reason for the photocatalytic degradation of the dye solution in the presence of Zn content sample, compared to the pure sample, is probably the non-crystallization of the cobalt oxide structure in the presence of Zn content calcined at 300 °C. For this reason, we will probably need to increase the calcination temperature for calcination of the doped sample.

A simplified Langmuir–Hinshelwood (L–H) kinetic model (Equation (3)) was used to describe the photocatalytic degradation rate of MB by plotting the graph of −ln(C/C0) versus time, t [23].

$$-\ln(C/C_0) = kt \quad (3)$$

where C_0 and C are the MB concentrations in solution at times 0 and t, respectively, and k is the apparent first-order reaction rate constant. In the above equation, k can be calculated by plotting $\ln(C_0/C)$ in terms of t and calculating its slope.

In this research, only the reaction rate constant (k) of the photocatalytic samples was calculated in the form of the following numbers. According to these numbers and results of photocatalytic activity, the doped sample (ZCH (10 % Zn)) has a higher rate constant, which is in accordance with the results of photocatalytic decomposition and is a confirmation of the results of photocatalytic decomposition.

Photocatalytic degradation (η) and apparent first-order reaction rate constant (k) of MB solution in the presence of ZCH (10 % Zn) sample calcined at 300 °C under visible light was investigated. Based on the obtained results, it can be concluded that if this parameter (k) takes a higher value, it will have better photocatalytic properties (CH-300 sample: k = 0.0086 min^{-1} and ZCH sample: k = 0.0034 min^{-1}).

Repetition test for the best sample with higher percentages of photocatalytic degradation (ZCH-300, 10 % Zn) was done for six times, the results of which are shown in Figure 6 that confirms the reuse of the catalyst nanoparticles doped with Zn cation (10 %) for the degradation of MB solution during an experiment for six repetitions. Each experiment was performed under the same conditions of initial concentration of 50 ml MB solution (10 ppm), 0.1 g ZCH with the Zn concentration of 10 mol %, and irradiation time of one hour.

The photodegradaion efficiency values were obtained as 10.6 %, 9.3 %, 8.2 %, 7.4 %, 7.1 %, and 6.7 % for the first to the sixth runs, respectively. Apparently, after the sixth time of the experiment, the percentage of photocatalytic destruction decreased by about 36 %, indicating that after each experiment repetition, a reduction was observed in the Photocatalytic degradation probably due to the deactivation of some active surfaces on the photocatalyst surface.

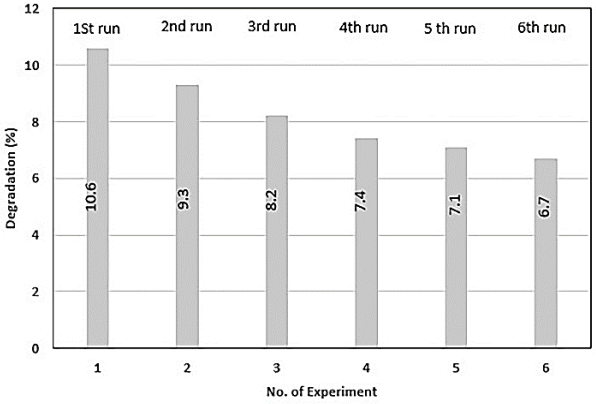

Figure 6. The reproducibility of the ZCH-300 catalyst for MB photodegradation for six cycles)

The optical band gap energies of the pure (CH-300) and doped samples (ZCH-300) calcined at 300 °C were measured as 1.39 eV and 1.48 eV, respectively. According to the FESEM results, addition of Zn content to the structure of cobalt oxide caused an increase in the E_g due to the smaller particle size in the presence of Zn content.

3.4. FESEM, EDS, and Maps Analysis of the CH and ZCH Samples

FESEM was used to study the morphology of the nanoparticles. FESEM photographs show the pure (Figure 7a,b) and doped (ZCH) samples (Figure 7c,d). Differences in the particle morphology were apparently observed followed by addition of Zn. According to the observations of the cobalt oxide morphology, the particles are irregular in shape; however, this observation is not true about the doped sample. Accordingly, it can be concluded that addition of Zn content increased the porosity and improved the particle morphology. The particle size in the pure cobalt oxide sample is in the range of 20-40 nm, and in the range of about 20-30 nm and in the doped sample whose morphology is quite porous. The average particle size of the calcined ZCH sample at 300 °C is smaller than that of the pure sample

due to the presence of the Zn content. The average particle size of the ZCH sample calcined at 300 °C is about 25 nm. The presence and distribution of elements in the ZCH (Figure 7e) sample calcined at 300 °C were analyzed using Energy Dispersive X-ray Spectroscopy (EDS). The EDS analysis confirmed the presence of cobalt, oxygen, and zinc in the synthesized ZCH sample.

According to the EDS mapping images illustrated in Figure 8, Cobalt (Figure 8a), oxygen (Figure 8b), and zinc (Figure 8c) are homogeneously distributed throughout the region. In particular, Zn is evenly distributed in the surface layers of cobalt oxide nanoparticles.

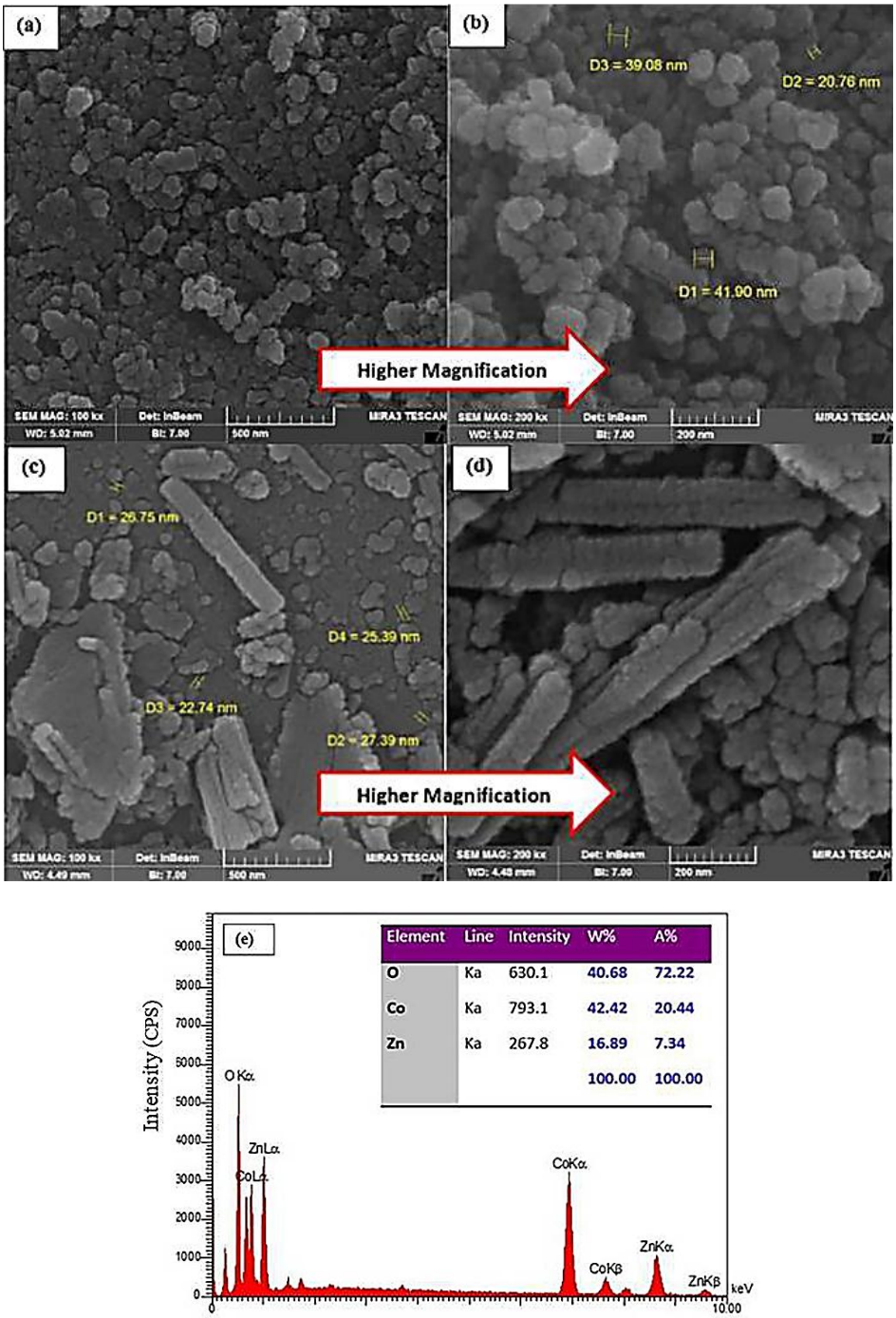

Figure 7. FESEM images of the as-prepared (a, b) Co_3O_4 nanoparticles (CH) and (c, d) ZCH samples at two magnifications, (e) EDS of ZCH-300 (10 % Zn)

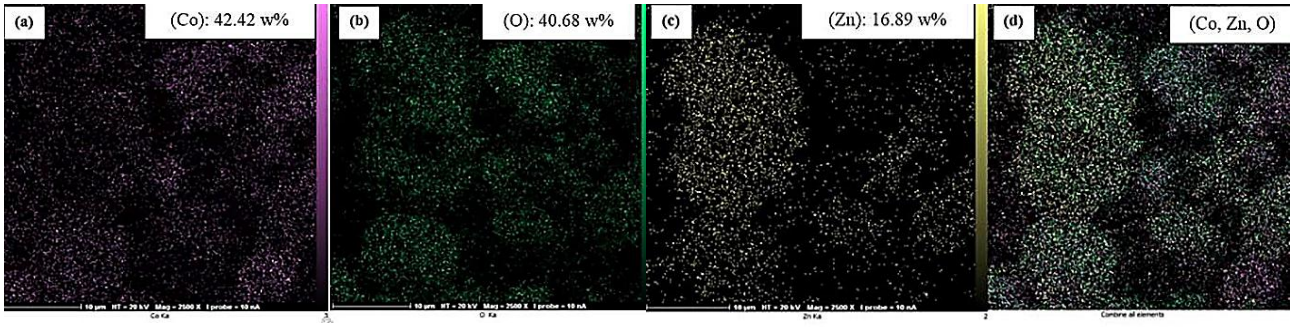

Figure 8. Map distribution of elements at ZCH-300: (a) Cobalt, (b) Oxygen, (c) Zinc, and (d) combine all elements

3.5 TEM Results

The TEM (inset: SAED) pattern depicted in Figure 9a consists of concentric rings, which correspond to (220), (311), and (400) planes of Co_3O_4 with cubic structure. Pure Co_3O_4 nanoparticles (CH) with higher magnification are shown in Figure 9b. According to this figure, the size of the nanoparticles is in the range of 20-30 nanometers. The TEM of the Zn doped Co_3O_4 nanoparticles (ZCH) is shown in Figure 9c. The particle size of the ZCH is in the range of 10-20 nm. Further, HRTEM of Co_3O_4 sample is shown in Figure 9d. In this figure, the distance between the layers (interlayer spacing) is about 0.24 nm and 0.28 nm, which corresponds to the planes with the Miller index (311) and (220) of the cube cobalt oxide structure, respectively.

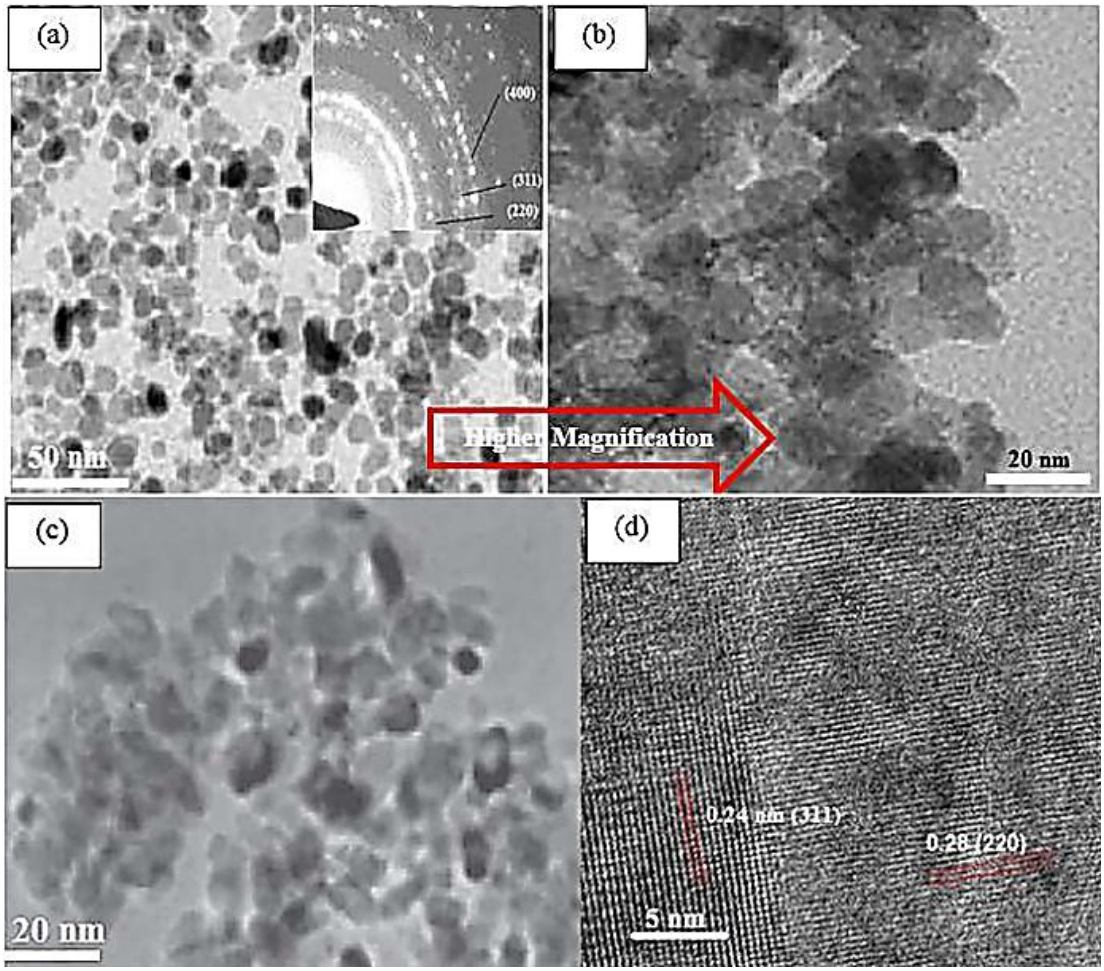

Figure 9. TEM image: (a,b) pure Co_3O_4, (c): Zn doped Co_3O_4(d) HRTEM of Co_3O_4 nanoparticles

4. CONCLUSIONS

In this research, cobalt oxide nanoparticles doped with Zn cations were synthesized by hydrothermal method. The effects of metal ion doping on the crystallizations of Co_3O_4 phase, crystallite size, and optical properties of CH mesoporous nanoparticles were investigated, and the following results were obtained.

- Addition of Zn content to the structure of Co_3O_4 nanoparticles reduced the crystalline size of samples.
- Addition of Zn content to the structure of cobalt oxide at the calcination temperature of 300 ºC led to an increase in the energy of the band gap from 1.39 eV to 1.48 eV mainly due to the smaller size of the particles in the presence of the Zn content.
- According to the FESEM images, the particle size of the pure sample was in the range of 20-40 nm and followed by addition of Zn content to the structure of pure cobalt oxide, the particle size (20-30 nm) decreased. In general, based on the obtained results, ZCH nanoparticles exhibited the best photocatalytical performance owing to a decrease in the electron-hole recombination rate and an increasing in the visible-light capturing.

ACKNOWLEDGMENTS

This study was funded by Malayer University. The authors highly acknowledge the financial support of Malayer University.

REFERENCES

1. Edla, R., Patel, N., Orlandi, M., Bazzanella, N., Bello, V., Maurizio, C., Mattei, G., Mazzoldi, P., Miotello, A., "Highly photo-catalytically active hierarchical 3D porous/urchin nanostructured Co_3O_4 coating synthesized by Pulsed Laser Deposition", ***Applied Catalysis B: Environmental***, Vol. 166, (2015), 475-484. https://doi.org/10.1016/j.apcatb.2014.11.060
2. Cole, K. M., Kirk, D. W., Thorpe, S. J., "Co_3O_4 nanoparticles characterized by XPS and UPS", ***Surface Science Spectra***, Vol. 28, No. 1, (2021), 014001. https://doi.org/10.1116/6.0000477
3. Abebe, E. M., Ujihara, M., "Influence of Temperature on ZnO/Co_3O_4 Nanocomposites for High Energy Storage Supercapacitors", ***ACS Omega***, Vol. 6, No. 37, (2021) 23750−23763. https://doi.org/10.1021/acsomega.1c02059
4. Manteghi, F., Kazemi, S. H., Peyvandipour, M., Asghari, A., "Preparation and application of cobalt oxide nanostructures as electrode materials for electrochemical supercapacitors", ***RSC Advances***, Vol. 5, No. 93, (2015), 76458-76463. https://doi.org/10.1039/C5RA09060A
5. Kalantarian, M. M., Asgari, S., "Theoretical Assessment of the First Cycle Transition, Structural Stability and Electrochemical Properties of Li_2FeSiO_4 as a Cathode Material for Li-ion Battery", ***Advanced Ceramic Progress***, Vol. 3, No. 4, (2017), 25-33. https://doi.org/10.30501/acp.2017.90762
6. Peng, J., Meng, J., Chen, D., Liu, H., Hao, S., Sui, X., Du, X., "A Review of Lithium-Ion Battery Capacity Estimation Methods for Onboard Battery Management Systems: Recent Progress and Perspectives", ***Batteries***, Vol. 8, No. 11, (2022), 229. https://doi.org/10.3390/batteries8110229
7. Niknam, E., Naffakh-Moosavy, H., Moosavifard, S. E., Afshar, M. G., "Multi-shelled bimetal V-doped Co_3O_4 hollow spheres derived from metal organic framework for high performance supercapacitors", ***Journal of Energy Storage***, Vol. 44, (2021), 103508. https://doi.org/10.1016/j.est.2021.103508
8. Ghobadi, N., Bahiraie, H., Kazazzi, M., "Effect of Ni Substitution on Optical Transitions and Magnetic Behavior of Mesoporous $Ni_xCo_{3-x}O_4$ ($0 \leq x \leq 1$) Thin Films Prepared by Electrophoretic Deposition", ***Journal of Electronic Materials***, Vol. 50, (2021), 987–991. https://doi.org/10.1007/s11664-020-08627-4
9. Zhao, X., Pang, Z., Wu, M., Liu, X., Zhang, H., Ma, Y., Sun, Z., Zhang, L., Chen, X., "Magnetic field-assisted synthesis of wire-like Co_3O_4 nanostructures: Electrochemical and photocatalytic studies", ***Materials Research Bulletin***, Vol. 48, No. 1, (2013), 92-95. https://doi.org/10.1016/j.materresbull.2012.10.001
10. Chen, Y., Hu, L., Wang, M., Min, Y., Zhang, Y., "self-assembled Co_3O_4 porous nanostructures and their photocatalytic activity", ***Colloids and Surfaces A: Physicochemical and Engineering Aspects***, Vol. 336, No. 1-3, (2009), 64-68. https://doi.org/10.1016/j.colsurfa.2008.11.018
11. Grzelczak, M., Zhang, J., Pfrommer, J., Hartmann, J., Driess, M., Antonietti, M., Wang, X., "Electro- and Photochemical Water Oxidation on Ligand-free Co_3O_4 Nanoparticles with Tunable Sizes", ***ACS Catalysis***, Vol. 3, No. 3, (2013), 383-388. https://doi.org/10.1021/cs3007523
12. Roy, M., Ghosh, S., Naskar, M. K., "Synthesis of morphology controllable porous Co_3O_4 nanostructures with tunable textural properties and their catalytic application", ***Dalton Transactions***, Vol. 43, No. 26, (2014), 10248-10257. https://doi.org/10.1039/C4DT00608A
13. Sun, H., Ang, H. M., Tadé, M. O., Wang, S., "Co_3O_4 nanocrystals with predominantly exposed facets: synthesis, environmental and energy applications", ***Journal of Materials Chemistry A***, Vol. 1, (2013), 14427-14442. https://doi.org/10.1039/C3TA12960H
14. Gasparotto, A., Barreca, D., Bekermann, D., Devi, A., Fischer, R.A., Fornasiero, P., Gombac, V., Lebedev, O.I., Maccato, C., Montini, T., Van Tendeloo, G., "F-Doped Co_3O_4 Photocatalysts for Sustainable H_2 Generation from Water/Ethanol", ***Journal of the American Chemical Society***, Vol. 133, No. 48, (2011), 19362-19365. https://doi.org/10.1021/ja210078d
15. Rosen, J., Hutchings, G. S., Jiao, F., "Ordered Mesoporous Cobalt Oxide as Highly Efficient Oxygen Evolution Catalyst", ***Journal of the American Chemical Society***, Vol. 135, No. 11, (2013), 4516-4521. https://doi.org/10.1021/ja400555q
16. Hitkari, G., Sandhya, S., Gajanan, P., Shrivash, M. K., Deepak, K., "Synthesis of Chromium Doped Cobalt Oxide (Cr:Co_3O_4) Nanoparticles by Co-Precipitation Method and Enhanced Photocatalytic Properties in the Visible Region", ***Journal of Material Sciences and Engineering***, Vol. 7, No. 1, (2018), 419. https://doi.org/10.4172/2169-0022.1000419
17. Ahmadi, M., Koozegar Kaleji, B., "TCA (Ag doped TiO_2-CuO) mesoporous composite nanoparticles: optical, XPS and morphological characterization", ***Journal of Materials Science: Materials in Electronics***, Vol. 32, No. 10, (2021), 13450-13461. https://doi.org/10.1007/s10854-021-05923-5
18. Che, H., Liu, A., Mu, J., Bai, Y., Wu, C., Zhang, X., Zhang, Z., Wang, G., "Facile synthesis of flower-like $Ni_xCo_{3-x}O_4$ ($0 \leq x \leq 1.5$) microstructures as high-performance electrode materials for supercapacitors", ***Electrochimica Acta***, Vol. 225, (2017), 283-291. https://doi.org/10.1016/j.electacta.2016.12.164
19. Koozegar Kaleji, B., Alijani, M., Aghaei, A., "Sn/Ce co-doping of TiO_2 nanoparticles: influence of dopants concentration on optical and structural characteristics", ***Journal of Materials Science: Materials in Electronic***, Vol. 27, (2016), 8524-8531.

https://doi.org/10.1007/s10854-016-4869-7

20. Hao, J., Peng, S., Li, H., Dang, S., Qin, T., Wen, Y., Huang, J., Ma, F., Gao, D., Li, F., Cao, G., "A low crystallinity oxygen-vacancy-rich Co_3O_4 cathode for high-performance flexible asymmetric supercapacitors", ***Journal of Materials Chemistry A***, Vol. 6, (2018), 16094-16100. https://doi.org/10.1039/C8TA06349D
21. Liu, J., Guan, C., Zhou, C., Fan, Z., Ke, Q., Zhang, G., Liu, C., Wang, J., "A flexible Quasi-solid-state nickel-zinc battery with high energy and power densities based on 3D electrode design", ***Advanced Materials***, Vol. 28, No. 39, (2016), 8732-8739. https://doi.org/10.1002/adma.201603038
22. Du, F., Zuo, X., Yang, Q., Li, G., Ding, Z., Wu, M., Ma, Y., Jin, S., Zhu, K., "Facile hydrothermal reduction synthesis of porous Co_3O_4 nanosheets@RGO nanocomposite and applied as a supercapacitor electrode with enhanced specific capacitance and excellent cycle stability", ***Electrochimica Acta***, Vol. 222, (2016), 976-982. https://doi.org/10.1016/j.electacta.2016.11.065
23. Mandić, V., Kurajica, S., Plodinec, M., Panžić, I., "Thermal Stability and Utilization of 1D-Nanostructured Co_3O_4 Rods Derived by Simple Solvothermal Processing", ***Catalysts***, Vol. 12, No. 10, (2022), 1162. https://doi.org/10.3390/catal12101162